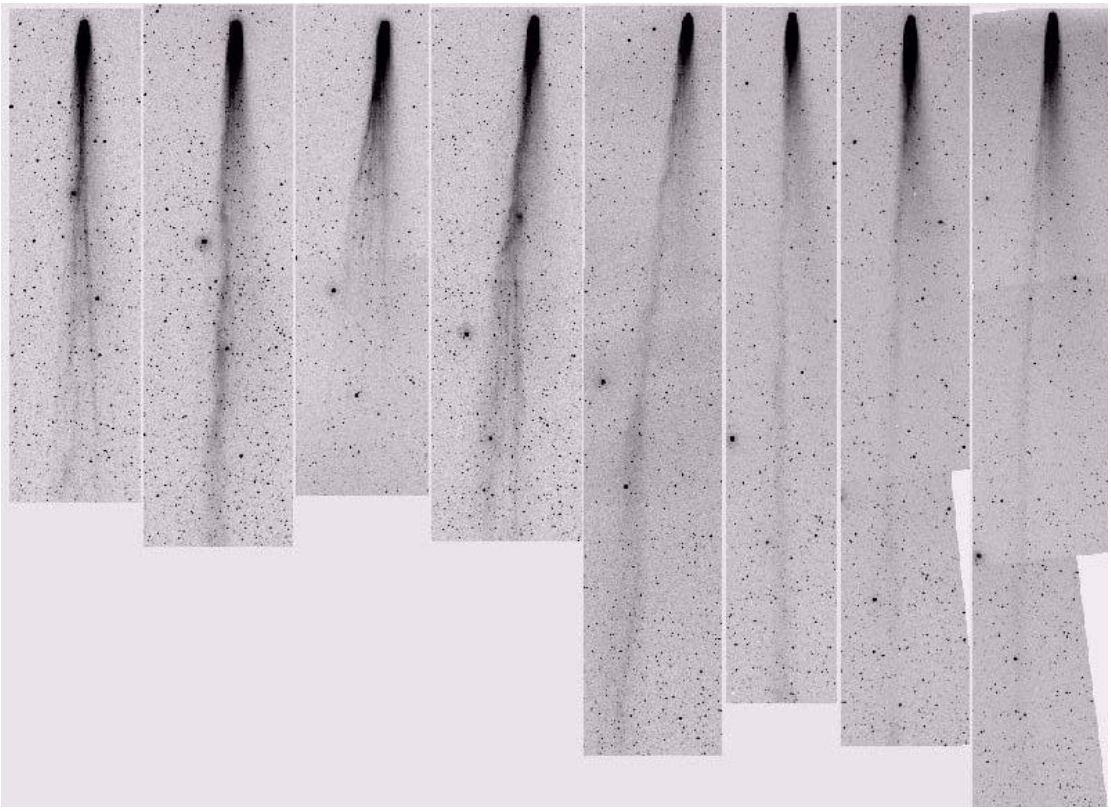

Chapter 3 The Solar Wind

A Basic Characteristics

The solar wind is the supersonic flow of plasma produced in the upper reaches of the solar atmosphere. This flow of plasma outward from the sun defines most of our 'space weather' - and hence it is essential to understand before we can study the near-earth satellite environment. The solar wind was hypothesized to exist on the basis of a number of pre-space age observations, including observations of comets. Spectral observations of comets show that the dusty tail of a comet is pointed in a direction consistent with solar photon pressure, arcing away from the sun as one might predict. The plasma tail points directly away from the sun, however, and can show startling structure. Figure 3.1 shows a nice illustration of the plasma tail of a comet.

Figure 3.1 image of comet Hale-Bopp, taken on 1997 Apr. 4 (19h44-19h56UT) with 20-cm, f/2 Baker-Schmidt camera and Fujicolor 400 SG+ film. The field of view is about 5x3.5 deg. Copyright © 1997 by B. Kambic & H. Mikuz.
http://www.fiz.uni-lj.si/astro/comets/images/95o1tcga-3.html

The composition of the solar wind is similar to the composition of the sun's upper atmosphere (~90% protons, ~10% He^{++}). The expansion speed is very slow in the inner corona, but increases rapidly outward, becoming supersonic at 10-20 solar radii. Here, supersonic means that the flow (or bulk) velocity of the solar wind is large compared to the average thermal velocity of the ions. (The ion mach number is greater than one). The characteristics of the solar wind at the earth's orbit (1AU from the sun) are given in Table 3.1.

Figure 3.2 illustrates most of the plasma properties at earth's orbit, for quiet times. The short term variability of the data seen here are fairly typical. Note that the electron bulk speed and ion speed should be very close - the electron measurement is a difficult one (by contrast to the ion measurement). Note the error bars on the electron measurement. Similarly, the proton and electron densities are relatively close, though one should keep in mind that quasi-neutrality only requires that the total ion charge density equal the electron density. Since there is a fair amount of He^{++} present, the proton density will nominally be about 90% of the electron density. By contrast, there is no overwhelming reason for the temperatures to be the same, though the variability in the values for ions again reflects the relative difficulty of the measurement - by contrast electron temperatures are fairly easy to obtain accurately.

Table 3.1

	Min Values	Average Values	Max Values
Flux (10^8 ions/cm^2 sec)	1.0	3.0	10
Velocity (km/sec)	300	468	700
Density (ions/cm^3)	3.2	6.5	20
Electron Temperature (K)	9,000	140,000	2×10^5
Proton Temperature (K)	10,000	50,000	3×10^5
Magnetic Field Strength (nT)	2.2	6.6	10

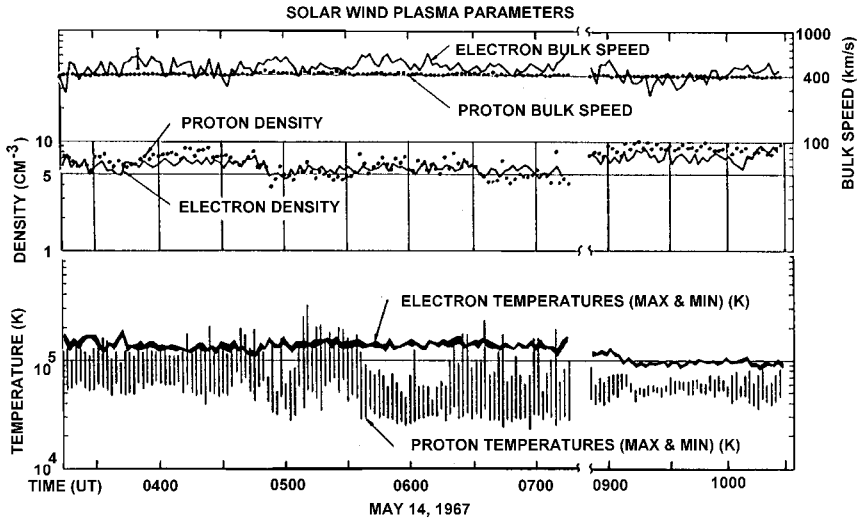

Figure 3.2 Solar wind plasma properties observed on Vela 4B
From: Montgomery, M. D., S. J. Bame, and A. J. Hundhausen, Solar Wind Electrons: Vela 4 measurements, *Journal of Geophysical Research, 73,* 4999, 1968.

The base values for the solar wind plasma illustrated above should not be considered all that typical. The variable nature of the solar wind plasma is illustrated by Figure 3.3, which shows a remarkable figure summarizing two decades of solar wind measurements, utilizing most of the data obtained during the space age. Data from 14 satellites are used, mapped to 1 AU (earth orbit). The data were smoothed using an 81 day running average, so fine scale events such as shock waves (section 3.5) are smoothed over.

These standard values will determine the standard size and shape of the earth's magnetosphere. Variations from these norms can result from solar activity, particularly flares. A major flare can cause a shock wave to be launched into the solar wind, doubling it's velocity. In addition to the hot plasma, there are also more energetic particles in the solar wind. These energetic particles extend up in energy to an MeV or more.

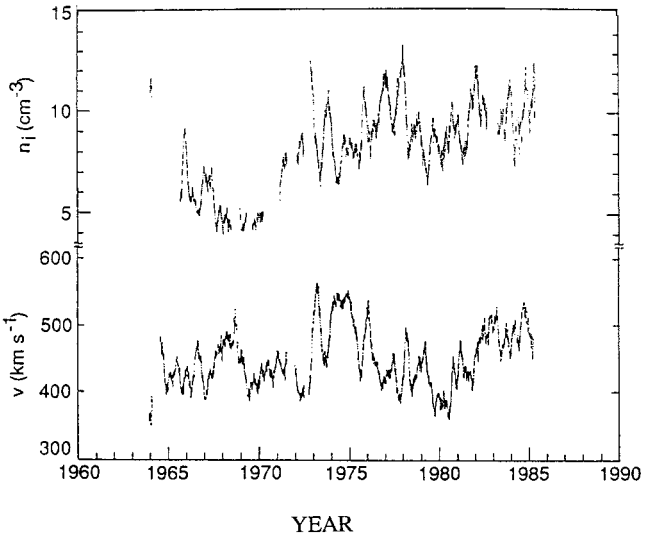

Figure 3.3 Solar wind ion density (top panel) and flow velocity (bottom panel) are shown for a 20 year period. Data are smoothed with an 81 day running average.

From: One year variations in the near earth solar wind ion density and bulk flow velocity, Scott J. Bolton, Geophysical Research Letters, vol. 17, p 37, 1990.

B The "Supersonic" Solar Wind

We begin with one of the first and most fundamental elements of the behavior of the solar wind. If the solar wind originates in the corona where the temperature is about 10^6 °K why is the solar wind velocity at 1 AU several times as high as the thermal velocities corresponding to the coronal temperatures? Figure 3.4 emphasizes this supersonic character of the solar wind. Charged particle data taken at 0.34 AU show ions with an energy/unit charge of about one keV, but the width (FWHM) is only a few tens of eV. The distributions are clearly supersonic.

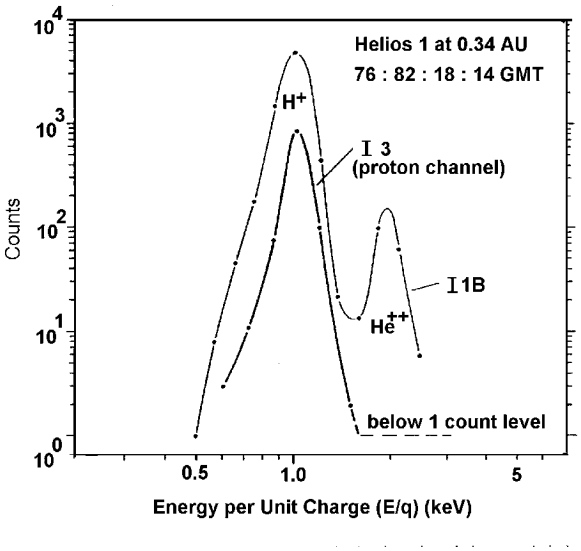

Figure 3.4 Count rate spectra simultaneously measured by the electrodynamic (mass analyzing) analyzer (I3)and electrostatic analyzer (I 1b). The primary peak in both spectra is due to protons; the secondary peak in the electrostatic analyzer is due to He++ (α) particles.

Rosenbauer, H., R. Schwenn, E. Marsch, B. Meyer, H. Miggenrieder, M. D. Montgomery, K. H. Mühlhäuser, W. Pilipp, W. Voges, and S. M. Zink, A Survey on Initial Results of the Helios Plasma Experiment, *Journal of Geophysics, 42,* 56-580, 1977.

The answer was obtained by Eugene Parker from the University of Chicago. He found that for a star like ours (e.g. one with the proper temperature) an acceleration of the outflowing gases to supersonic speed can occur. The process has been compared to the gas flow through a rocket nozzle (De Laval Nozzle) which also results in supersonic flow under the proper conditions. If the temperature of the corona is very low we have essentially a static atmosphere (such as the earth's) with very little escape of gas. The density in such an atmosphere is given by the barometric relation:

$$n(r) = n_o \exp\left[\frac{G M_\odot m_H}{kT R_\odot}\left(\frac{1}{r} - \frac{1}{r_0}\right)\right] \qquad \text{(Eqn. 3.1)}$$

n is the plasma density at r; n_o is the plasma density at r_o;
r_o is the reference altitude in solar radii, nominally 1 solar radius;
m_H is the mass of the proton (hydrogen nucleus) (in kg),
T is the temperature of the corona (in K or eV);
k is the Boltzmann constant; 1.38×10^{-23} J/K if T is in K, otherwise use k = 1.6×10^{-19} J/eV;
G is the gravitational constant,
M_o is the mass of the Sun (in kg); R_o is the radius of the sun (in meters)

If we now increase the temperature so that the atmospheric gases begin to escape into space we note that the total mass flow through any concentric sphere must be a constant (conservation of mass). We can write this as:

$$\rho(r)\, V_r\, 4\pi\, r^2 = m\, n(r)\, V_r\, 4\pi\, r^2 = \text{a constant} \qquad \text{(Eqn. 3.2)}$$

where V_r = radial velocity, $\rho = nm$ is the mass density.

We see from the form of n(r), or $\rho(r)$, that it will decrease very sharply within the first few solar radii, depending on T, of course. (Homework problem 3.7). If the density falls off faster than $1/r^2$ (which it does) then V_r must <u>increase</u> to maintain constant mass flow. Thus we can achieve velocities higher than the speed of sound in the medium, or supersonic flow. If the temperature

gets very large then $\rho(r)$ is approximately constant and V_r has to decrease as we go further out. Thus very hot stars presumably show a stellar "breeze" whose speed decreases as we go outward. Once outside a distance of 5 or 10 solar radii, the acceleration process has ended, and the solar wind reaches an equilibrium velocity.

Figure 3.5 shows how the solar wind is observed to vary in density and flow velocity with distance from the sun. These data from 1978 were taken from Helios 1 and Voyager 1, from 0.3 to 1.0, and 1.0 to 5 AU, respectively. Over the observed range, the solar wind velocity is roughly constant at 400 km/s - the fluctuations seen here are a reflection of solar activity, as with figure 3.3.

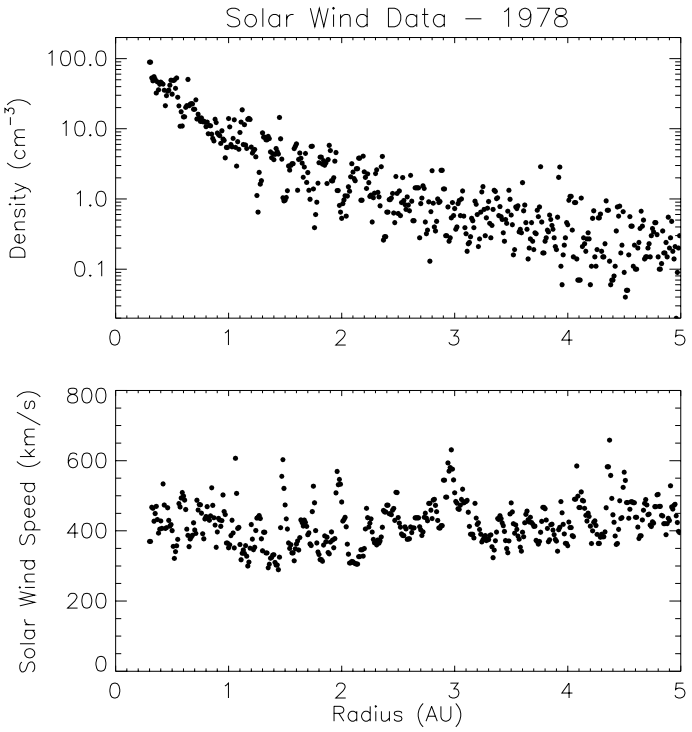

Figure 3.5 Solar Wind data from 1978, acquired from NSSDC for Helios 1 and Voyager 1.

C The Interplanetary Magnetic Field (IMF)

As we saw above, the plasma and the solar magnetic field form a closely coupled system. In the inner corona (out to about 3 $R_\odot$) the magnetic field energy density dominates the kinetic energy density. This fact causes the inner corona to corotate with the sun like a rigid body (see Figure 3.6). This is possible since the magnetic fields can transfer angular momentum to the coronal plasma.

Beyond $3R_\odot$ the magnetic energy density falls off faster than the kinetic energy density of the plasma. At this point the outward moving plasma falls behind the sun's rotation and drags the magnetic field lines with it forming an Archimedes spiral structure. This process is somewhat analogous to the pattern formed by a rotating sprinkler and the angle between the radial direction and the field line is often referred to as the garden hose angle ψ (see Figure 3.6). At the orbit of the earth the garden hose angle ψ is about 45° and is given by

$$\tan \Psi = \omega_\odot \, r / V_{sw} \qquad \text{(Eqn. 3.3)}$$

where $\omega_\odot$ is the angular velocity of the sun $\left(2.7 \times 10^{-6} \text{ radians/second}\right)$, r is the radial distance and V_{sw} is the speed of the solar wind particles. This formula was predicted by Eugene Parker (University of Chicago) before the advent of the space age, and the eventual confirmation of this relation is one of the great triumphs of space plasma theory. A simplified derivation follows here.

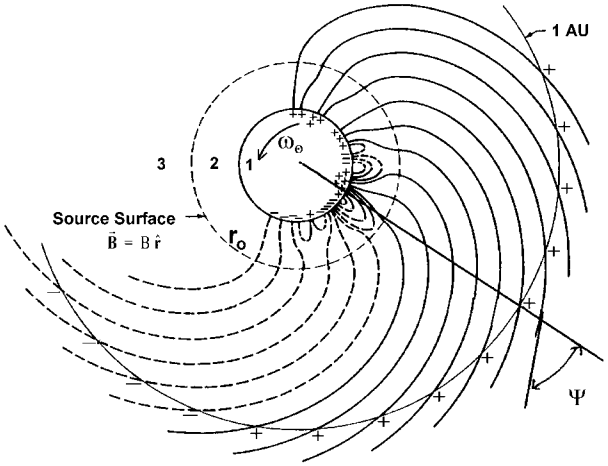

Figure 3.6 Spiral Structure of the solar wind. Three regions are defined here:
The solar surface, where the photospheric magnetic field can be obtained, as from observations at Mount Wilson.
The acceleration region, where the magnetic field can be calculated from potential theory

$$\left(\nabla^2 \phi = 0\right)\left(\text{ or } \nabla \times \mathbf{B} = 0\right)$$

Steady state region - magnetic field transported by solar wind as observed by satellites. $\dfrac{d\vec{B}}{dt} = -\vec{B}\left(\nabla \bullet \vec{V}\right) + \left(\vec{B} \bullet \nabla\right)\vec{V}$

Figure modified from that found in Schatten, K.H., J. M. Wilcox, N. F. Ness, A model of interplanetary and coronal magnetic fields, Solar Physics, 6, pages 442-455, 1969.

We obtain our defining equation by considering a snapshot of the charges leaving the solar surface at some time t, and then integrate this equation in order to obtain the locus of charges in space. Note that this is not the trajectory of any individual charged particle. Just as in the water hose analogy, each particle is instantaneously moving radially away from the sun. Figure 3.7 illustrates the geometry to be used.

Figure 3.7 Geometry for IMF derivation

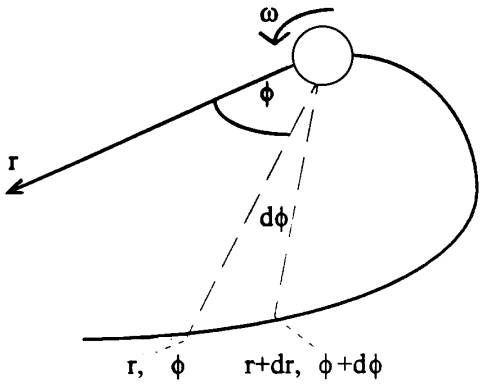

$\omega_\odot$ = angular velocity of the sun
r_o = 3 solar radii, the effective radius of the corona
V_{sw} = solar wind velocity

Now:
Let r, ϕ be the coordinates of the particle at a time, t, and r+dr, ϕ+dϕ be the coordinates of particle 2 at the same time.
Let t_o be the time at which particle 1 left the corona, t_o+dt_o be the time at which particle 2 left the corona.

Then: $t - t_o = \frac{r - r_o}{v_{sw}}$; $dt_o = \frac{d\phi}{\omega_\odot}$, and $t - (t_o + dt_o) = \frac{r + dr - r_o}{v_{sw}}$

combining these we obtain: $dr = -\frac{v_{sw}}{\omega_\odot} d\phi$

This can be integrated to obtain:

$$\int_{r_o}^{r} dr = -\frac{v_{sw}}{\omega_\odot}\int_{\phi_o}^{\phi} d\phi \qquad \text{(Eqn. 3.4)}$$

which is easily evaluated to be:

$$r - r_o = -\frac{v_{sw}}{\omega_\odot}(\phi - \phi_o) \qquad \text{(Eqn. 3.5).}$$

Here, r_o, ϕ_o describes the position of the charge element at t = 0. We can make use of a fortuitous combination of numerical values, and then abandon mks units. Noting that the nominal value for the solar wind velocity is 400 km/s, we obtain:

$$\frac{v_{sw}}{\omega_\odot} = \frac{4\times10^5 \frac{m}{s}}{2.69\times10^{-6} \frac{radians}{s}} = 1.5\times10^{11} \text{ m=1 AU} \qquad \text{(Eqn. 3.6)}$$

Further noting that r_o << r for all observations made on satellites (r_o is a few solar radii), and that we have the freedom to take ϕ_o as zero, we obtain a very simple formula:

$$r\,(AU) = -\phi \qquad \text{(Eqn. 3.7)}$$

Referring back to Figure 3.7, we note that ϕ is measured in radians, and we are using the customary convention that the positive ϕ direction is counter-clockwise. Since r is positive, it is apparent that ϕ is a negative number - the spiral is pointed clockwise.

It can be shown that the radial component of the spiral IMF must decrease as r^{-2}, and we then have for the two components and magnitude of **B**:

$$B_r = B_{r_o}\left(\frac{r_o}{r}\right)^2, \text{ and } B_\phi = -\frac{\omega_\odot\, r}{v_{sw}} B_r = -B_{r_o}\frac{\omega_\odot\, r}{v_{sw}}\left(\frac{r_o}{r}\right)^2 \qquad \text{(Eqn. 3.8)}$$

$$B = \sqrt{B_r^2 + B_\phi^2} = B_{r_o}\left(\frac{r_o}{r}\right)^2\sqrt{1+\frac{\omega_\odot^2\, r^2}{v_{sw}^2}} \qquad \text{(Eqn. 3.9)}$$

The agreement of this model with in situ measurements is displayed in Figures 3.8 and 3.9, respectively.

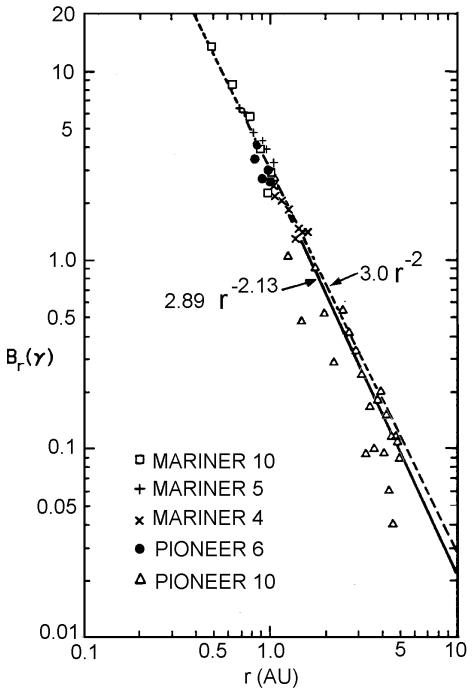

Figure 3.8 (left) Solar rotation averages of the magnitude of the IMF radial component B_r measured by Mariner 4, 5, and 10 and Pioneer 6 and 10. Curves showing and r^{-2} radial distance dependence (dashed curve) and the 'best' least squares fit to the combined data (solid curve) are included. From: Behannon, K., Heliocentric distance dependence of the Interplanetary Magnetic Field, Reviews of Geophysics and Space Physics, 16, 125-144, 1978
Magnetic field variation with distance from the sun

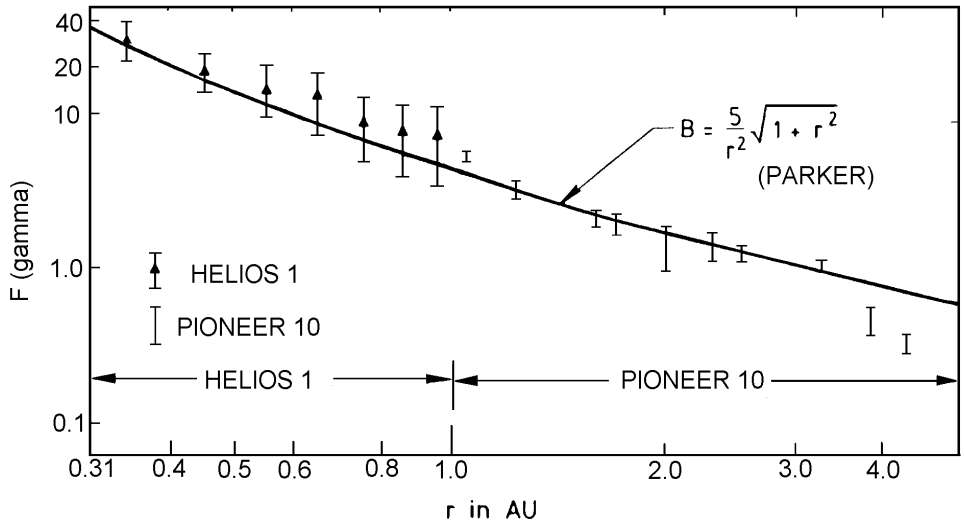

Figure 3.9 Range and central value (black triangle) of magnetic flux (F) in gamma (1 γ = 1 nano-Tesla, or 1 nT) for distance bins of 0.1 AU versus distance from the sun. Data are from Helios-1 and Pioneer 10. The fitted curve is from Parker's theory. G. Musmann, F. M. Neubauer, and E. Lammers, Radial Variation of the Interplanetary Magnetic Field between 0.3 and 1.0 AU, Observations by the Helios-1 Spacecraft, *Journal of Geophysics, 42,* 591-598, 1977

Finally, we see from figure 3.6 that the garden hose angle ψ is given by:

$$\tan \Psi = \frac{B_\phi}{B_r} = \frac{\omega_\odot r}{v_{sw}} \qquad \text{(Eqn. 3.10)}$$

as given at the beginning of this section. At 1 AU, tan $\psi \approx 1$, and $\psi \approx 45°$. This latter value is verified by observations, as shown in Figure 3.10. This summary of a decade of observations was obtained from the National Space Science Data Center (NASA/NSSDC) archives. Hourly observations were summarized here, binned in one degree increments. The figure indicates a peculiar problem, however. The expected observations are occurring at ψ=45°, but there is a second peak at 225°. The former is due to magnetic fields pointed outward from the sun, the latter to inward pointing fields. Parker's theory is silent on this problem - the distinction is in the source region on the sun's surface. Why would there be such a variation?

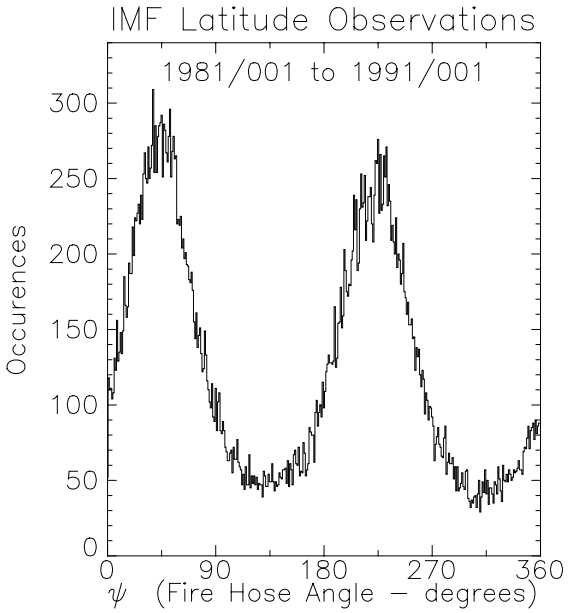

Figure 3.10 Solar Wind magnetic field data taken at earth orbit from 1981-1990.

D Sector Structure

The quandary noted above regarding the direction of the IMF was noted early in IMF field observations. Figure 3.11 shows a summary of a few early orbits of the IMP platform. The inward/outward duality was noticed to organize itself by solar rotation. Near the solar equatorial plane the interplanetary magnetic field (IMF) is organized into sectors or regions (typically four to six) where the magnetic field is predominantly directed either away from or toward the sun as shown in Figure 3.11. It was initially thought this structure reflected the longitudinal structure of the sun's surface field. It is now believed that this observational pattern reflects the relative motion of the earth, and its satellites, above and below the magnetic field lines which map to the sun's magnetic equator.

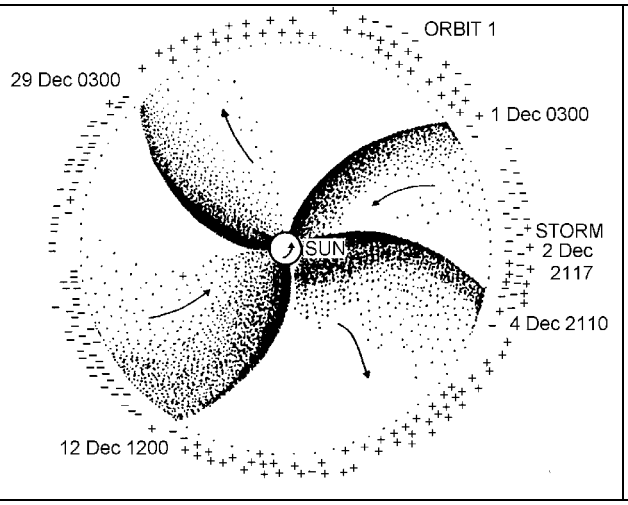

Figure 3.11 Solar magnetic sector structure inferred from measurements from the Interplanetary Monitoring Platform (IMP) (Wilcox and Ness, 1965). Plus signs (away from the sun) and minus signs (toward sun) are 3 hour averages.

This sector structure is thought of as the result of the earth (effectively) moving above and below the sun's magnetic equator as the sun rotates. The 'heliospheric current sheet' is the boundary between the magnetic hemispheres of the sun. This boundary is uneven, and has been described (by Hannes Alfven) as somewhat like the ruffled skirt of a ballerina. As this structure sweeps past the earth, the earth moves above and below the plasma originating from the sun's magnetic equator. This is the origin of the dual values for the 'garden hose' angle.

The current sheet is a natural consequence of having oppositely directed magnetic fields in the two solar hemispheres - a similar feature will be found in the earth's magnetosphere. This interpretation was largely proven correct by the recent Ulysses mission, which saw the disappearance of the sector structure as the satellite left the ecliptic plane, and circled the sun in a polar orbit; (E. J. Smith et al, Disappearance of the Heliospheric Sector Structure at Ulysses, Geophysical Research Letters, 20, page 2327, November 5, 1993)

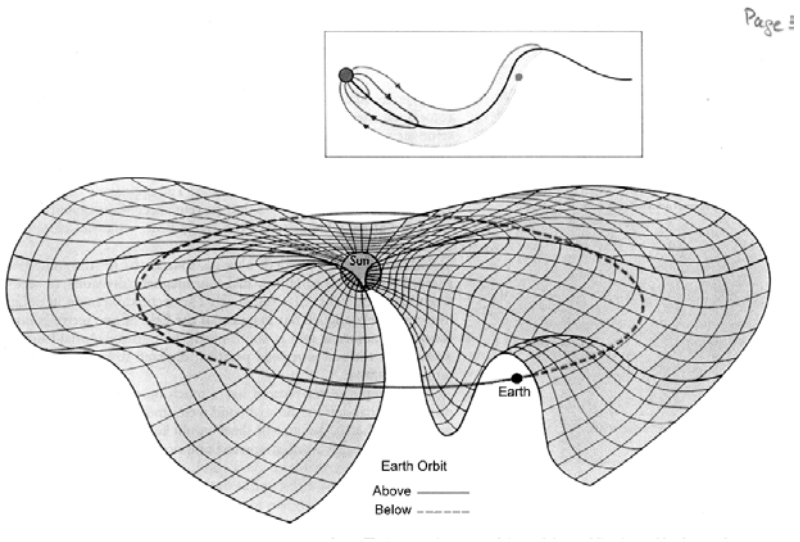

Figure 3.12 The Heliospheric current sheet.

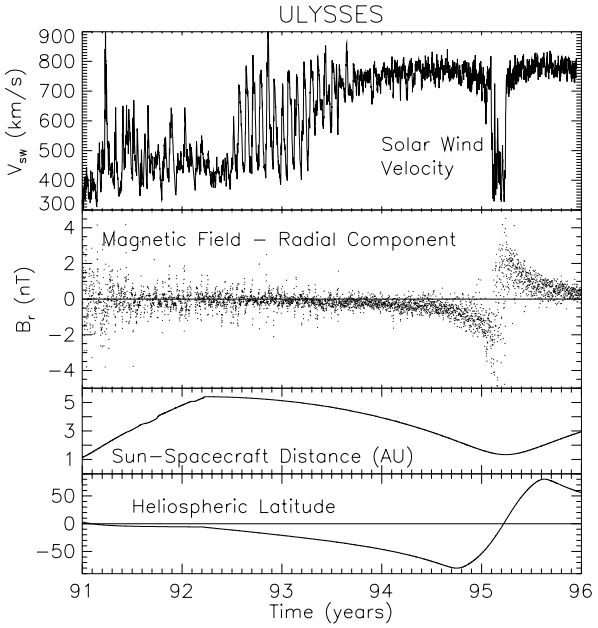

Figure 3.13. Summary of 5 years of data from the Ulysses SWOOPS instrument, obtained from the European Space Agency. The satellite cruised relatively slowly out to Jupiter (at 5 AU), then turned south and out of the ecliptic plane. Nearly four years after launch by the space shuttle Discovery, on 13 September 1994, the European-built spacecraft reached the most southerly point on its out-of-ecliptic orbit, 80.2 degrees south of the Sun's equator, at a distance of 2.3 astronomical units (345 million km) from the Sun. Less than a year later, the satellite passed over the north solar pole, reaching a peak latitude of 80.2°.

Note that above ~40° solar magnetic latitude, only high speed solar wind is observed, and that as the satellite moved below the ecliptic plane, primarily negative values of Br were found. In 1995, at northern latitudes, positive values are found.

Data obtained from the European Space Agency (ESA) Ulysses archive. See URL http://helio.estec.esa.nl/ulysses/. The above result was first published by: J. L. Phillips, A. Balogh, S. J. Bame, B. E. Goldstein, J. T. Gosling, J. T. Hoeksema, D. J. McComas, M. Neugebaure, N. R. Sheely, and Y.-M. Wang, Ulysses at 50° south: Constant immersion in the high-speed solar wind, Geophysical Research Letters, 21, page 1105, 1994. Also, Ulysses Explores The South Pole Of The Sun, R.G. Marsden, ESA Bulletin No.82 May 1995)

E The Source of the Fast Solar Wind

The reality of the solar wind origin ended up being somewhat more complex than Parker's theory, particularly because of the complex magnetic field structure near the solar surface. Frequently, the solar wind speed would be observed to increase dramatically to ~800 km/s. The so-called "fast" solar wind streams were ultimately recognized as being a high-solar latitude phenomena, as discussed above. The evolution of observations and theory currently indicate that the solar wind must originate from regions called coronal holes – that is regions which appear dark in extreme ultraviolet (EUV) and x-ray images. In 1999 this general understanding was dramatically changed by the work of Hassler et al, illustrated below. Using the SOHO satellite imagers, they were able to deduce that the specific origin was at the boundaries defined by the chromospheric network, corresponding roughly to the edges of the cells defined by super-granulation.

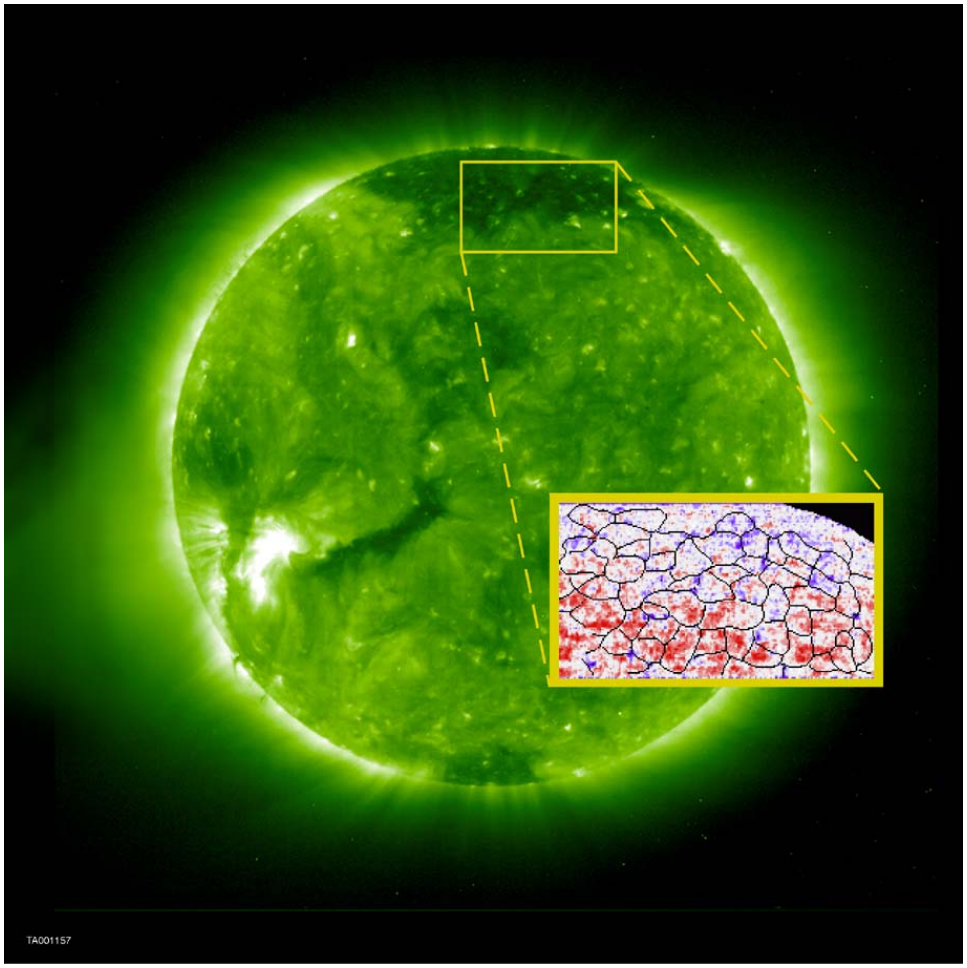

Figure 3.14 Extreme ultraviolet image of the Sun taken with the EAS/NASA Solar and Heliospheric Observatory (SOHO) Spacecraft revealing gas at 1.5 million degrees shaped by magnetic fields. Bright regions indicate hot, dense plasma loops with strong magnetic fields, while dark regions imply an open magnetic field geometry (coronal hole), and are the source of the high speed solar wind. Hassler et al, Solare Wind Outflow and the Chromospheric Magnetic Network, *Science, 283,* page 810, February 5, 1999. Photo Credit: ESA/NASA
http://www.boulder.swri.edu/~hassler/SW_press_release.html

Figure 3.14 shows a solar image from 22 September 1996 (near solar minimum) taken at 195 Å, imaging FE XII at an approximate temperature of 1.5 million K. The "zoomed-in" or "close-up" region shows a Doppler velocity map of million degree gas at the base of the solar atmosphere, where the solar wind originates. This image is obtained from SUMER Ne VIII 770 Å line-of-sight Doppler velocity measurements, on a scale ranging from ± 10 km/s Blue represents blue shifts or outflows and red represents red shfts or downflows. The atmospheric motion toward us, away from the solar surface, is seen as a blue shift, and is the beginning of the solar wind. The blue regions are inside the coronal hole, or open magnetic field region, where the high speed solar wind is accelerated. Superposed at the edges of the cells is the chromospheric network, where the strongest flows (dark blue) occur.

F Interplanetary Shocks

The largest fluctuations in the solar wind are the solar flare induced shock waves. Interplanetary shocks are responsible for magnetic storms on the earth, and ultimately, major anomalies in satellite operations. The explosion of plasma in the lower corona termed the solar flare, launches a shock wave which propagates at 800-1000 km/s outward into the solar wind. (Note, following the discussion at the end of chapter 2, it is perhaps most accurate to relate the shock wave to coronal mass ejections (CME's). There still seems to be a majority opinion that CME's are due to flares, however.)

Figure 3.14 shows a cartoon view of a shock. There is a shock front, which consists of hotter, denser plasma, with enhanced magnetic fields. Behind this shock front is the driver gas, which may have enhanced levels of alpha particles (He^{++}). This latter feature is thought to be a significant clue as to the nature of the flare process.

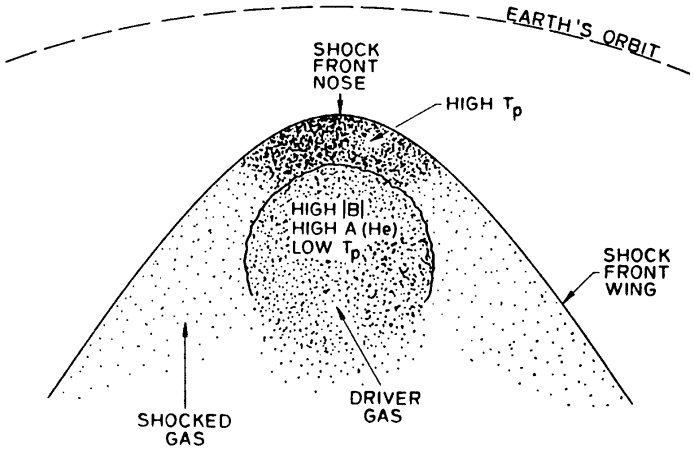

Figure 3.14 Cartoon for interplanetary shock approaching earth orbit. From: An analysis of shock wave disturbances observed at 1AU from 1971 through 1978, G. Borrini, J. T. Gosling, S. J. Bame, and W. C. Feldman, Journal of Geophysical Research, vol. 87, page 4365, 1982.

A sense of the kinds of changes that normally occur is given by Figure 3.15a, which shows an averaged view of 103 shocks observed by IMP6, 7, and 8, at 1 AU, from 1971 to 1978. The shock front takes less than a day to pass the earth; this is the period during which the magnetosphere will be most dramatically affected. Figure 3.15b shows a complementary view of the same process, using Pioneer 11 data, and a much finer time scale. It can be seen that the

leading edge transition is very sharp, and in this case the shock front passed the satellite fairly quickly (several AU downstream from earth).

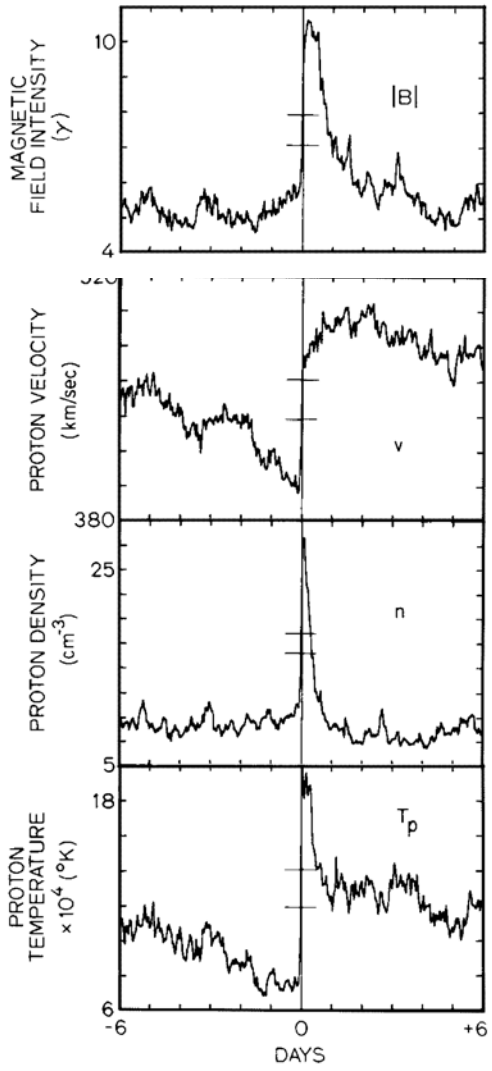

Figure 3.15a Superposed epoch plots of solar wind proton velocity, density, temperature, and magnetic field intensity, for 103 shock events at 1 AU. One-hour averages of data are employed. The small horizontal error bars indicate the normal variance of each parameter.

From: An analysis of shock wave disturbances observed at 1AU from 1971 through 1978, G. Borrini, J. T. Gosling, S. J. Bame, and W. C. Feldman, Journal of Geophysical Research, vol. 87, page 4365, 1982.

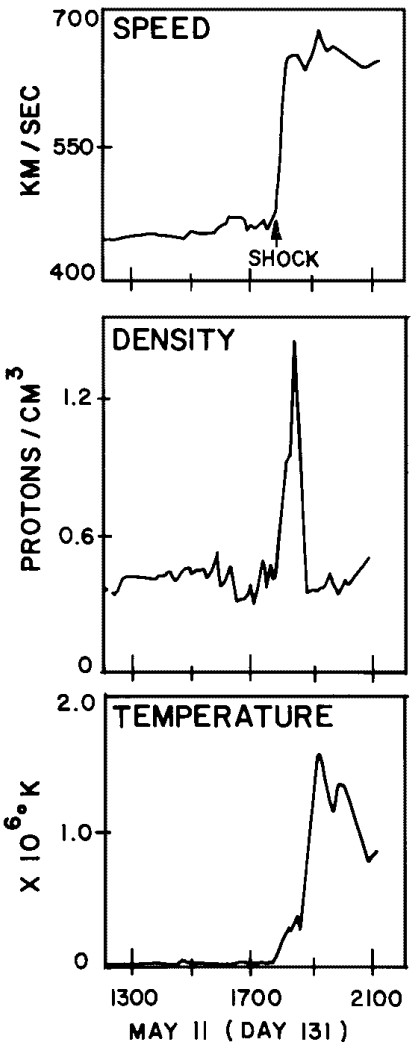

Figure 3.15b Plasma data from Pioneer 11, on May 11, 1978.

From: Plasma shocks and energetic particles in the outer solar system: Trapping and Asymmetry observations from Pioneer 10 and Pioneer 11, D. S. Intrilligator and W. D. Miller, Journal of Geophysical Research, vol. 87, page 4354, 1982.

G References

Akasofu, S. I. Interaction between a Magnetized Plasma Flow and a Strongly Magnetized Celestial Body with an Ionized Atmosphere: Energetics of the Magnetosphere, Annual Review of Astronomy and Astrophysics, Vol. 20, p 117, 1982.

Falthammer, C. G.. The Solar Wind, in Cosmical Geophysics, Egeland et. al. eds. Universitetsforlaget, Oslo Sweden, Chapter 7, 1973.

Hill, Thomas W. and Wolf, Richard A., Solar Wind Interactions in The Upper Atmosphere and Magnetosphere. National Sciences, Washington, D. C., p 25, 1977.

Hollweg, J. V. The Energy Balance of the Solar Wind, in The Sun as a Star, NASA Monograph, NASA SP-450., 1981.

Hundhausen, A. J., Coronal Expansion and Solar Wind. Springer-Verlag, N. Y., 1972.

Kopp, R. A. (1981) Heating and Acceleration of the Solar Wind, in The Sun as Star, NASA Monograph, NASA SP-450.

Wilcox, J. M. and Ness, N. F. (1965). Quasi-Stationary Corotating Structure in the Interplanetary Medium. J. Geophys. Res., 70, 5793.

H Problems

1. Calculate Beta (β) for the solar wind. Note that you need to modify the form used earlier just a bit, since this is a streaming plasma, with a velocity v:

$$\beta = \frac{\text{Kinetic Energy Density}}{\text{Magnetic Energy Density}} = \frac{\frac{1}{2} nmv^2}{B^2 / 2\mu_o}$$

2. Suppose, using the new space telescope we detect that a nearby hot star has a stellar wind flowing at 600 km/sec. Could we say that this stellar wind is supersonic? Explain.

3. If the solar wind speed doubles, how will the spiral (or "garden-hose angle") change? Does this situation ever occur? Explain.

4. Compare the solar wind particle density at the time of solar minimum with the particle density at solar maximum. Does the solar wind speed change during the solar cycle? Explain.

5. What does it mean to say that the "solar wind is supersonic"? Calculate ratio of the ion flow velocity to the average kinetic (thermal) energy of a 7 eV proton. This is the (ion) Mach number. Repeat for the solar wind electrons (T ~ 10 eV).

6. Waves can travel along magnetic field lines much like waves travel along a stretched string. The speed of these "magnetic" waves (called Alfven waves) is given by

$$V_A = \sqrt{\frac{B^2}{\rho \mu_0}}$$

where B is the magnetic field strength, ρ is the plasma density, and μ_0 is the magnetic permeability. Is the solar wind super-Alfvenic (i.e. faster that V_A)? If so, why is this important? Is this in any way analogous to being supersonic?

7. Use equations 31 and 3.2 to obtain V_{sw} as a function of r for the region from near the sun's surface out to 2 $R_\odot$, for 3 possible temperatures. Take m = hydrogen mass (1 amu), T = 1,000,000 K, 1,500,000 and 2,000,000 K (1.0, 1.5, and 3.0 million degrees), $\rho = 10^{-10}$ gm / cm^3 at r = $R_\odot$, and V_o = 1 km/s. The solar wind reaches supersonic velocity in this region. Show the mach number is greater than 1. ($\mathcal{M} > 1$) at 2 $R_\odot$, for the solutions you generate.

$$\left(M = \sqrt{\tfrac{1}{2} m v_{sw}^2 \,/\, \tfrac{3}{2} kT} \;=\; v_{sw} / \sqrt{3kT/m} \;=\; v_{sw} / v_{thermal} \right)$$

Figure 3.16 shows the complete solution to the expansion problem as formulated by Parker. (Your result will not look like this.)

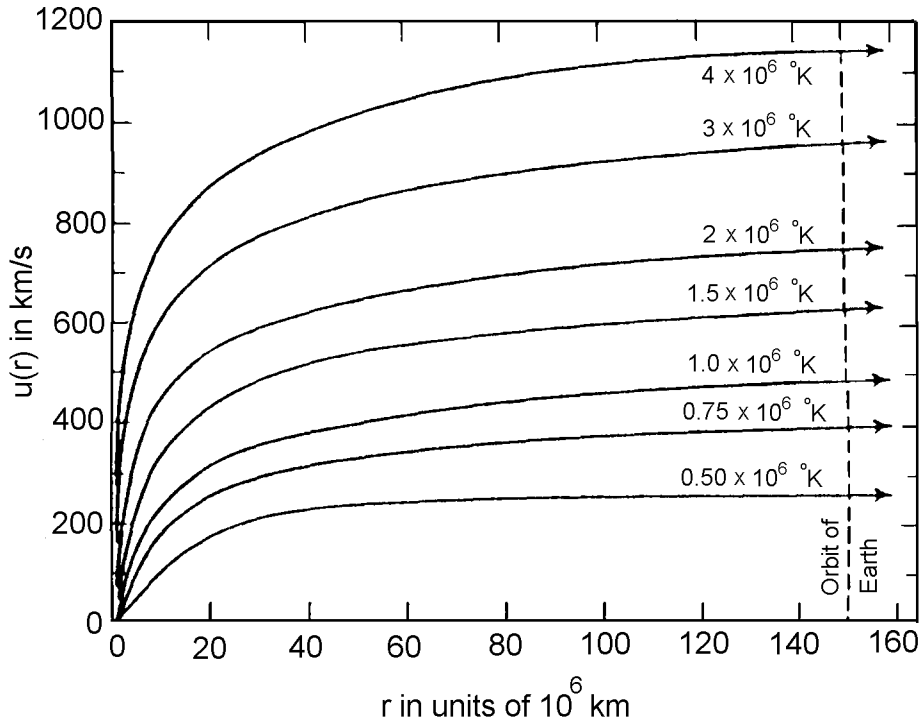

Figure 3.16 Expansion speed (u(r)) as a function of heliocentric distance for isothermal coronas of various temperatures.
Originally done in: E. N. Parker, Dynamics of the Interplanetary Gas and magnetic Field, *Astrophysical Journal, 128,* pages 664-676, 1958.
This version found in: A. J. Hundhausen, Coronal Expansion and Solar Wind, New York, Springer-Verlag, 1972, citing in turn Parker, E. N., Interplanetary Dynamical Processes, New York, Interscience Publishers, 1963.

This page intentionally left blank